Influence of the Bombarding Ion Energy and Surface Composition on the Ground-state Atom Fraction in Solids Analysis using Multiphoton Resonance Ionization

David L. Pappas,† David M. Hrubowchak,‡ Matthew H. Ervin and Nicholas Winograd*
Department of Chemistry, The Pennsylvania State University, 152 Davey Laboratory, University Park, PA 16802, USA

Multiphoton resonance ionization (MPRI) is used to probe the desorption characteristics of ion-bombarded surfaces of Fe, In and Ni. The effects of primary ion kinetic energy and surface chemistry on the sensitivity and accuracy of MPRI detection are examined. The relative Ni^*/Ni° and In_2°/In° ratios are found to increase as the energy of the incident Ar^+ ion is varied from 300 eV to 1000 eV. A reflecting time-of-flight mass spectrometer is employed to collect efficiently the photoions as well as secondary ions, permitting accurate determination of the ground-state atom fraction and thereby completing a detailed fundamental analysis of the analytical capabilities of the MPRI approach. The ground-state atom fractions are found to parallel changes in surface composition and represent 30–90% of the material desorbed from ion beam-cleaned and air-exposed Fe and In matrices. In contrast, the corresponding secondary ion fractions vary over several orders of magnitude and are difficult to correlate with surface chemistry.

INTRODUCTION

The recently reported detection limit of a few hundred surface atoms has demonstrated the extreme sensitivity of multiphoton resonance ionization (MPRI) of ion beam-desorbed matter.[1] The additional advantages in quantitation and selectivity over established techniques for surface characterization have enabled improved analyses of traditionally difficult systems.[2,3] Although the application of the MPRI approach is expected to encompass an expanding variety of surface analytical challenges, continued realization of its capabilities requires detailed examination of the individual factors which govern the measured response.

Analytical methodologies involving detection of ion-desorbed material are often described in terms of the useful yield or number of ions detected per atom desorbed.[4,5] The useful yield is typically a measured quantity which is generally effective for characterizing the overall efficiency of an analysis. However, it provides little insight on the details associated with the measurement of fundamental surface desorption phenomena. Such information is obtained only through examination of the independent variables which contribute to the useful yield. Among these are the instrumental parameters, which define the collection and counting efficiencies and have already been addressed in some detail for the MPRI experiment.[6] The remaining factor influencing the useful yield is the partitioning of the surface atoms into the ionic, neutral, atomic and molecular species that are observed in the vapor flux. The most abundant of these, the neutral atoms, are known to leave the surface in varying degrees of electronic excitation. Many of the occupied energy levels may not be conveniently probed by state-selective resonance ionization. The number of atoms in the electronic state of interest, relative to the total quantity of desorbed matter, is termed the useful fraction. The state of interest is typically the ground level, which normally contains the largest population. Few attempts have been made at determining true useful fractions for MPRI since a rigorous analysis requires either detection of all desorbed species, including each of the populated atomic electronic states, or pre-existing knowledge of the absolute sputter yield and the instrument transmission and detection efficiencies. None the less, the useful fraction is the most significant descriptor of MPRI detection. For example, since it is a measure of the number of countable particles, it establishes a practical upper limit for the sensitivity. In addition, insight on the behavior of the useful fraction permits prediction of the effects of changes in the experimental parameters on the measured quantities and facilitates correlation of those measurements with the surface composition. Finally, since it is determined strictly by the process of ion-induced desorption, the useful fraction provides a direct means for characterization of that process. Once the useful fraction has been determined, it may be combined with the remaining experimental variables (ionization efficiency, collection efficiency, instrument transmission) to calculate the useful yield for various experimental configurations. This provides an effective measure for comparing MPRI with a variety of techniques employing bombardment-induced desorption, both from an empirical standpoint as well as a practical perspective.[7–12] Two such methods considered here are

* Author to whom correspondence should be addressed.
† Present address: IBM Research, T. J. Watson Research Center, PO Box 218, Yorktown Heights, NY 10598, USA.
‡ Present address: GTE Products Corp., 655 S. Willow St., Manchester, NH 03103, USA.

0142-2421/92/110743-08 $09.00

Received 28 August 1991
Accepted 4 June 1992

secondary ion mass spectrometry (SIMS) and non-resonant multiphoton ionization (MPI).[13,14]

One parameter which may affect the useful fraction is the energy of the primary ion. The specific kinetic energy selected for the incident particle often depends upon the analytical objective. For example, for measuring depth distributions, the bombardment energy is limited to a few hundred electron-volts or less in order to minimize atomic mixing in the solid. In contrast, trace measurements are enhanced through the use of large ion current densities normally achievable at high incident energy (>5 keV) to remove substantial amounts of the substrate.

Another factor which may influence the useful fraction is the surface chemical composition. For SIMS it is well established that the useful fraction or ionized desorbed fraction is strongly dependent upon the sample chemistry, thereby limiting the level of experimental accuracy.

In this work, we examine the influence of the surface condition (cleanliness) and primary ion energy on the useful fraction in the MPRI analysis of In, Fe and Ni solids. Indium is studied for its importance as a semiconductor dopant. Iron is examined for its significance as an impurity in Si devices and for comparison with other investigations of the electronic-state partitioning as measured by laser-induced fluorescence and MPRI under different experimental conditions.[9,15,16] Nickel is selected because of the dense manifold of low-lying metastable levels comparable in energy to those of other atoms studied previously.[17,18]

We find that the relative excited-state yields for Ni and the dimer/monomer fractions for In increase to a small extent as the incident ion energy is varied from 300 to 1000 eV, thus indicating a limited reduction in the useful fraction. Using the reflecting time-of-flight mass spectrometer, we are able to measure the useful fractions and electronic-state partitioning for Fe and In as a function of the surface chemistry. The ground-state atom fraction is found to be 0.3–0.5 for Fe and 0.7–0.9 for In, for desorption from air-exposed and clean surfaces, respectively. The corresponding secondary ion yields are lower and do not reflect the surface concentrations. Using the useful fraction data, the useful yields for MPRI of In are calculated to be 0.03 (air-exposed) and 0.04 (clean), indicating that the sensitivity of MPRI may be up to two orders of magnitude greater than that of MPI and four orders of magnitude greater than that of SIMS.

EXPERIMENTAL

The experimental apparatus is described in detail elsewhere.[6,19] Two ion sources are available for these studies. For low incident energies (200–1000 eV), a 20 nA Ar^+ ion beam is delivered into a 1–5 mm diameter spot in 3–5 μs pulses. For higher kinetic energy measurements, a 10 keV Ar^+ ion beam (50 μA, 5.6 μs pulses, 3 mm diameter spot) is employed. All primary ions are incident at 45°.

The laser system consists of a pair of dye lasers, pumped by the second harmonic of a Nd:YAG laser. Ionization of In and Ni is carried out using a single dye laser containing Exciton DCM dye/methanol solutions. The spectroscopic pathways through which In is studied have been previously indicated.[20] Summarizing, when the ground state is probed via the one-color $^2P^o_{1/2} \leftrightarrow {}^2S_{1/2} \rightarrow In^+ + e^-$ process, direct comparison may be made with the broadly resonant dimer (410 nm, 4.2 mJ $pulse^{-1}$, 2.5×10^6 W cm^{-2}). Concurrent measurement of the In ground and fast excited state ($^2P^o_{3/2}$, 2212.56 cm^{-1}) is accomplished via the two-color scheme employing $^2P^o_{1/2} \leftrightarrow {}^2D_{3/2}$ (303.8 nm) and $^2P^o_{3/2} \leftrightarrow {}^2D_{3/2}$ (325.9 nm) resonances, and ionization with 607.6 nm and 651.6 nm photons, respectively.

The relevant Ni spectroscopy is indicated in the partial electronic structure diagram shown in Fig. 1. Each two-step process requires a single wavelength (310–326 nm) and one resonant excitation. The laser provides 20–25 mJ $pulse^{-1}$ (1.3×10^7 W cm^{-2}) in the 600–650 nm range and 1–3 mJ $pulse^{-1}$ (1.2×10^6 W cm^{-2}) for the 300–326 nm radiation. The area of the unfocused beam above the sample is varied from 0.3 to 0.9 cm^2.

For ionization of Fe, a scheme requiring two independently tunable beams is employed. This is illustrated in the schematic energy-level diagram presented in Fig. 2. The three-step process proceeds through sequential resonances of the type $^5D \leftrightarrow {}^5F^o \leftrightarrow {}^5D$, followed by ionization. To generate the required beams, the Nd:YAG output is divided by a 70%/30% beam-splitter. The more intense component is used to pump a soluton of Kiton Red 620 dye/methanol. The dye output is then directed into the frequency doubling module to produce 0.5–1 mJ (4.4×10^5 W cm^{-2}) of 295–297 nm light used for the first Fe resonance. The 30% pump beam is utilized in a second dye laser containing Rhodamine 590 dye/methanol to yield 5–10 mJ (4.4×10^6 W cm^{-2}) of 564–569 nm radiation used for the second resonance

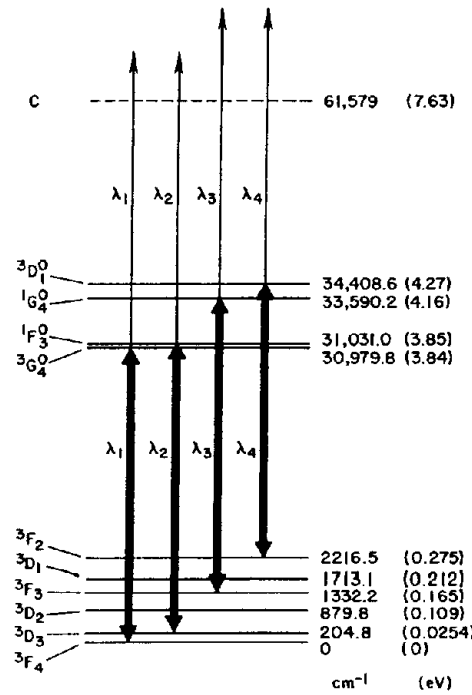

Figure 1. Partial electronic energy-level diagram for Ni, indicating the levels probed and transitions used: $\lambda_1 = 322.8$ nm; $\lambda_2 = 324.4$ nm; $\lambda_3 = 310.0$ nm; $\lambda_4 = 310.6$ nm.

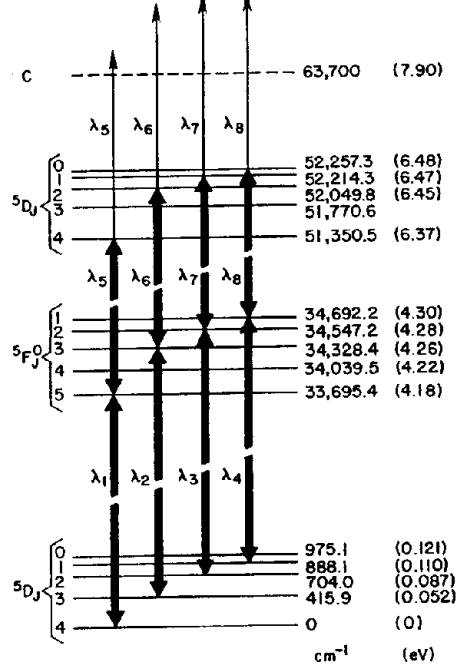

Figure 2. Partial electronic energy-level diagram for Fe, indicating the levels probed and transitions used: $\lambda_1 = 296.8$ nm; $\lambda_2 = 294.9$ nm; $\lambda_3 = 295.5$ nm; $\lambda_4 = 295.8$ nm; $\lambda_5 = 566.4$ nm; $\lambda_6 = 564.3$ nm; $\lambda_7 = 566.0$ nm; $\lambda_8 = 569.3$ nm.

transition. The two tunable beams are combined outside of the vacuum chamber and a variable delay line is employed for pulse synchronization. This approach allows high-power visible light to be used for the final ionization step, facilitating achievement of saturation conditions.

The vacuum system is equipped with three mass spectrometers. For the studies on the effect of the incident ion kinetic energy, for which absolute ion and neutral yield comparisons are not required, the photoions are collected into a simple low-resolution time-of-flight (TOF) device. This consists of an extractor positioned parallel to the sample surface at a distance of 3.8 cm, a 4.0 cm drift region and a Galileo 4038 channeltron electron multiplier detector. The low-resolution TOF configuration is sufficient for separating photoionized atoms from clusters and from the more energetic secondary ion packet. SIMS spectra are collected with an Extranuclear 162-8 quadrupole mass spectrometer equipped with an energy prefilter. Single ion counting in the SIMS mode is carried out with a Princeton Applied Research 1121A amplifier/discriminator and 1112 photon counter/processor.

For useful fraction measurements, it is necessary to measure the photoions and secondary ions at equivalent extraction and transmission efficiencies. This is accomplished with a reflecting TOF mass spectrometer, which provides second-order energy focusing while maintaining high transmission.[21] By varying the electrostatic reflection potentials, the device may also be used as an energy discriminator for reduction of background noise.[22] The drift chamber contains a number of optics for adjusting ion trajectories. Detection is carried out with a Galileo FTD 2002 microchannel plate assembly.

Polycrystalline In, Ni and Fe targets (Alpha Products; 99.999%, 99.998% and 99.998% purity, respectively) are used. After mechanical polishing, the In and Ni foils are immersed in an etch solution of 30% HNO_3, 10% H_2SO_4, 10% H_3PO_4 and 50% glacial CH_3COOH for 30 s. The Fe substrates are etched in a solution of 80% H_2O_2 (30%), 15% distilled H_2O and 5% HF for 30 s.

For the variable energy experiments, the targets are first cleaned by the defocused dc ion beam. The cleaning process is monitored using SIMS. Next, the desired bombardment energy is established in the pulsed ion beam mode and the response of each species is measured by signal averging for 30 s with a Stanford Research Systems SR 250 gated integrator and boxcar averager. This procedure is then repeated for each kinetic energy examined.

For the useful fraction determinations, targets designated as 'air-exposed' are inserted into the chamber and analyzed directly, with signal integration for 30 s for each atomic state. This is immediately followed by a measurement of the secondary ion yield. Ion bombardment of the entire surface (Ar^+, 50 μA, 5 min) is then carried out using the defocused dc beam, after which the measurements are repeated as before on the freshly 'cleaned' surfaces. Repetitive analyses are made by using multiple samples cut from the same foil and removing the targets from the chamber for re-exposure to the air. Note that although the peak ion current during the pulse is quite high, the duty cycle of $\sim 10^{-4}$ limits the total quantity of surface matter removed during the experiment to $\sim 10^{-2}$ monolayers. Thus, the measurement itself does not greatly disturb the surface morphology.

A number of corrections are applied to facilitate direct comparison of the ionic and neutral species in calculation of the useful fraction. First, since secondary ion yields are measured using a 982 ns primary ion pulse width, the SIMS data are normalized using the integrated MPRI/SIMS ion beam pulse area ratio. Also, the neutral atom data are adjusted to account for the fraction of atoms spatially overlapped (24.7% for the 5.6 μs ion beam pulse) with the photon field. The derivation of this correction is described elsewhere.[6] In addition, the assumption of equivalent extraction efficiency is made. Finally, the data for In are normalized to the known fluence (0.042 J cm^{-2}) required for ionization saturation.[6]

RESULTS AND DISCUSSION

Influence of primary ion energy on the useful fraction

The variation of the useful fraction with the incident ion kinetic energy is examined here using Ni and In. The Ni atom provides an effective example for illustrating the potential difficulties of the state selective process. There are five metastable energy levels within 0.3 eV of the ground state, but only three of these can be conveniently examined using the same laser dye employed for detection of the ground level. The signal intensities for each ionization process are found to exhibit a linear dependence on laser power, and saturation is not achieved. Since each state is detected using different

intermediate levels, the ionization probability out of which is unknown, only relative yields are reported.

The variation in the yield of desorbed ground-state Ni atoms ($^3F_4$) with incident Ar^+ energy is shown in Fig. 3. As the energy is increased from 600 eV to 1000 eV, the measured intensity rises by a factor of 1.8. However, the corresponding yields in the $^3F_3$ (1132.2 cm^{-1}) and $^3F_2$ (2216.5 cm^{-1}) levels increase at greater rates. Specifically, the $^3F_3/^3F_4$ and $^3F_2/^3F_4$ ratios (Fig. 4) rise by factors of 3.9 and 4.7, respectively. The relative yield of the lowest metastable state, $^3D_3/^3F_4$ (not shown), demonstrates no appreciable change.

Since the respective ionization processes are not saturated and the $^3D_2$ (879.8 cm^{-1}) and $^3D^1$ (1713.1 cm^{-1}) populations are not measured, accurate calculation of the useful fraction for Ni is not possible. Of the states

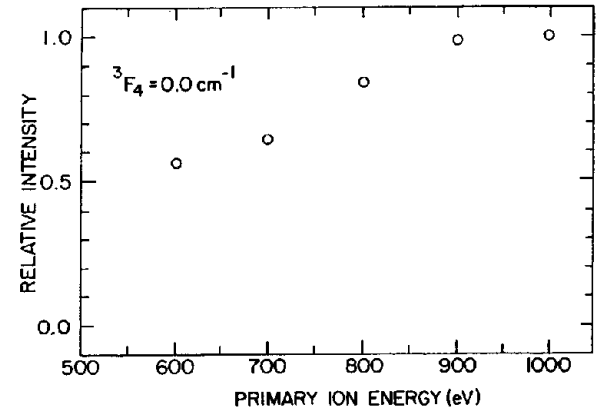

Figure 3. Normalized intensity of Ni ground electronic state ($^3F_4$) *vs.* primary Ar^+ ion kinetic energy.

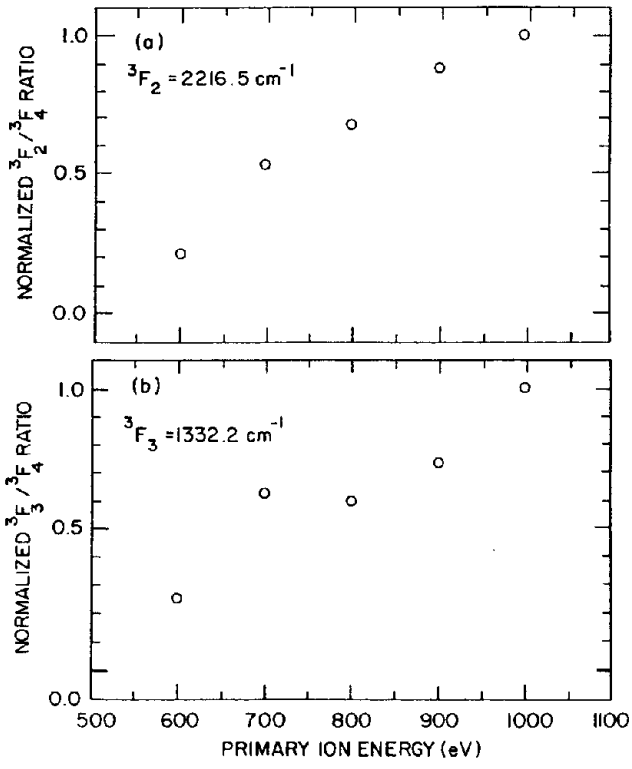

Figure 4. (a) Normalized ratio of Ni fifth excited electronic-state ($^3F_2$, 2216.5 cm^{-1}) and (b) third excited electronic-state ($^3F_3$, 1332.2 cm^{-1}) intensity to ground-state intensity as a function of primary Ar^+ ion kinetic energy.

which are examined, well over 90% of the summed experimental intensity is derived from the ground and first excited level, with approximately equal partitioning between the two. Since the yield of each is invariant with respect to the other over the energy range surveyed, the useful fraction would exhibit little apparent variation. However, if the relative fractions of the unmeasured states are significant and behave as do the $^3F_3$ and $^3F_2$ levels, then the useful fraction would decrease as the incident kinetic energy is raised. From the data, we estimate a ground-state useful fraction of <0.4 for desorption from a clean surface.

Although the electronic partitioning of ion-desorbed Ni has not been widely examined, the data can be related to studies of other atoms with excited states comparable in energy to those examined here. For example, in an investigation of ion-desorbed Zr using laser-induced fluorescence (LIF), it was found that the metastable components of the ground-state multiplet (570 cm^{-1}, 1240 cm^{-1}) exhibit five- to tenfold increases in population relative to that of the ground level as the bombarding Kr^+ ion energy is varied from 750 to 3000 eV.[17] Investigating a higher primary ion energy regime, Kimock reported that excited/ground fractions for In and Co rise in varying degrees with incident ion kinetic energy until reaching a plateau region, while the Al first excited state demonstrates no measurable change as compared with the ground state over the energy range 2–12 keV.[18] Interestingly, the lowest Al level lies only 112 cm^{-1} above the ground state, while the Ni first excited state is found at 204.7 cm^{-1}. The total energy required to reach a plateau may be minimal for both. In contrast, the Ni third (1332 cm^{-1}) and fifth (2216 cm^{-1}) excited levels are similar in energy to In and Co levels which require in excess of 4 keV incident beam energy to reach an apparent maximum in population relative to the ground state. An investigation of the degree of Ni excitation generated at these elevated bombarding energies might prove useful.

Regarding the mechanisms responsible for these observations, it is evident that the measured intensities reflect a combination of effects which populate/depopulate an electronic level prior to photoionization. It is known that at the kinetic energies investigated here, particle desorption is the result of momentum transfer through collisions.[23] The increase in beam energy can be viewed as a deposition of additional energy into this collision process, raising the probability of populating elevated electronic states. An alternative explanation for the observations might be that the rate of rise to the plateau in the excited/ground ratio is simply a function of the number of readily accessible states. For In and Al, there is only one level within 0.5 eV of the ground state, while for Ni and Co there are a number of energy levels within that range.

Indium offers the unusual opportunity for direct comparison of the resonantly ionized monomer and dimer. Since small molecules are usually difficult to detect by MPRI, not only does their behavior remain uncharacterized but the magnitude of their effect on the useful fraction is unknown. Such a limitation might be significant for complex matrices. Indium metal represents a simple system; In_2 is the only molecule observed with any significant intensity in the SIMS spectrum. None the less, the results may be illustrative

of more generalized phenomena. Since the ionization efficiency of the dimer is unknown, the data were collected at constant laser power and only relative yields are reported.

The relative desorbed dimer/monomer ratio obtained in sampling a clean In surface with a 300–1000 eV Ar^+ ion beam is presented in Fig. 5. The dimer fraction exhibits a small increase at low energies, followed by an apparent plateau. For comparison, results from measurement of the In_2^+/In^+ secondary ion yields have been included. No significant difference between the ion and neutral cluster behavior is observed.

A similar study has been performed by Gerhard and Oechsner, in which the behavior of several different elements was examined using desorbed neutral particle post-ionization in a low-pressure, high-frequency plasma.[24] A wide range of results were obtained, but several of the dimer/monomer *vs.* ion energy functions were found to parallel the curves of Fig. 5. Although the specific mechanism for this behavior cannot be determined from the data presented here, the observations show agreement with the results of classical dynamics calculations.[25] Further insight might be gained through energy- and angle-resolved measurement of the monomer and dimer distributions.

Calculation of the neutral dimer fraction from these data is not possible, since the dimer has been found to photodissociate at the detection wavelength.[26] In fact, most of the atoms observed in the $In^*(^2P_{3/2})$ state are photofragments. It is estimated from SIMS measurements that the In_2^+ yield is ~1% of the In^+ intensity at 1000 eV incident energy. Since the dimer-derived $^2P_{3/2}$ population is ~8% of the total yield (see next section) at 10 keV Ar^+ energy, it is apparent that the dimer/monomer ratio continues to rise at primary ion energies above 1000 eV. Thus, a second mechanism leading to a decrease in the useful fraction is confirmed. However, the magnitude of the effect is relatively small and only the production of heteronuclear molecules remains unexamined as a potential means for substantial alteration of the useful fraction in MPRI analysis of In.

Measurement of the useful fraction

Determination of the useful fraction for the MPRI experiment requires measurement of:

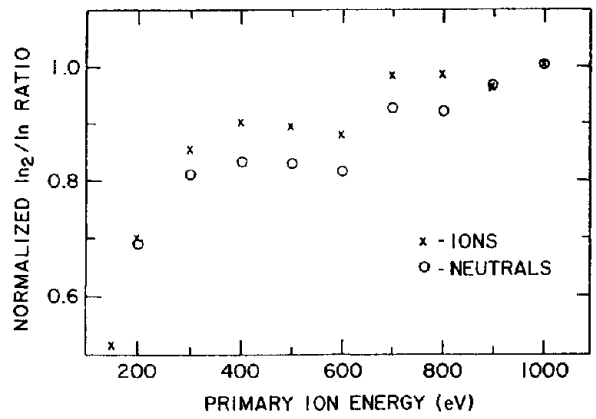

Figure 5. Normalized ratio of In_2 to In intensity as a function of primary Ar^+ ion kinetic energy, measured using quadrupole SIMS (×) and time-of-flight MPRI (○).

(1) all population atomic energy states;
(2) the molecular yield;
(3) the secondary ion yield.

For Fe and In, the first criterion is satisfied by probing the ground state and all low-energy metastable states under conditions of 100% ionization, or by correction to the known power density required for 100% ionization. The second criterion is assumed to be satisfied since SIMS analyses indicate that molecular species represent a small fraction of the total ion yield from the matrices examined here. The assumption of similar behavior for the neutral particles is justified on the basis of classical dynamics calculations of ion-induced desorption from metallic surfaces, which show that dimers are formed primarily by atomic recombination over the surface and that the mechanism for the formation of small cluster ions is similar to that of the molecular neutrals.[23] The third condition is met through the use of the reflecting TOF mass spectrometer along with the correction factors detailed in the experimental section.

The yield of each Fe electronic state exhibits a linear increase with power in the ionizing photon, followed by a plateau region. Saturation of the first resonance step is verified by blocking the visible light and obtaining the additional power curves for the subsequent one-color MPRI process, which also display a one-photon dependence.

The relative intensities and fractional yields of Fe species desorbed from air-exposed and ion beam-cleaned Fe solids (10 keV Ar^+ ion bombardment) are listed in Table 1. For desorption from the clean surface, Fe^+ and Fe^o fractions of 3.6×10^{-2} and 0.51, respectively, confirm the distinct improvement in sensitivity available with MPRI, as compared with SIMS. For the air-exposed sample, the desorbed particle reservoir contains approximately equal concentrations of ionized and neutral atoms. However, the MPRI useful fraction parallels the increase in surface Fe concentration which results from the cleaning procedure, while the Fe^+ ion flux drops. The sevenfold summed neutral ($Fe^o + Fe^*$) increase is larger than would be expected to result from simple oxide removal and may reflect contamination of the uncharacterized air-exposed surface. A change in the absolute sputter yield as a function of the oxygen concentration, another type of matrix effect, may also play a role, as has been experimentally observed.[27]

The electronic partitioning of the ^5D_j multiplet of Fe desorbed from the same matrices is presented in Table 2. Note that, for both targets, the largest channel for neutral atom ejection is the ground state. Comparison between these results and those of other experiments is

Table 1. Measured intensity and fractional yield of iron atomic species desorbed from air-exposed and ion beam-cleaned iron foils (Fe^*_{tot} refers to the sum of the four excited levels, ^5D_j ($j = 0$–3), of the ground-state manifold)

	Air-exposed		Clean	
Species	Intensity	Fraction	Intensity	Fraction
Fe^o	2.4 ± 0.6	0.34	18 ± 11	0.51
Fe^*_{tot}	2.6 ± 0.7	0.38	16 ± 11	0.45
Fe^+	2.0 ± 0.8	0.29	1.3 ± 0.8	3.6×10^{-2}

Table 2. Electronic partitioning of ion beam-desorbed Fe atoms as a function of surface contamination (air-exposed *vs.* ion beam-cleaned) and incident ion kinetic energy

State	Energy (cm^{-1})	Fractional yield: Air-exposed[a] 10 keV Ar^+	Fractional yield: Clean[a] 10 keV Ar^+	Fractional yield: Clean[b] 900 eV Ar^+
$^5D_4$	0	0.47	0.53	0.68
$^5D_3$	416	0.30	0.30	0.20
$^5D_2$	704	0.15	0.12	0.088
$^5D_1$	888	0.083	0.046	0.034

[a] This work.
[b] From Ref. 14.

Table 3. Measured intensity and fractional yield of indium atomic species desorbed from air-exposed and ion beam-cleaned indium foils [$In^*(^2In_{3/2})$ response is primarily due to photodissociation of In_2]

Species	Air-exposed: Intensity	Air-exposed: Fraction	Clean: Intensity	Clean: Fraction
$In^\circ(^2P_{1/2})$	79 ± 15	0.72	535 ± 180	0.92
$In^*(^2P_{3/2})$	17 ± 2	0.15	47 ± 16	0.081
In^+	15 ± 4	0.13	2.2 ± 0.8	3.8×10^{-3}

facilitated through calculation of an effective 'temperature' characterizing the desorbed population as described by the Boltzmann equation. For the atoms removed from the contaminated target under 10 keV Ar^+ ion bombardment, the population distribution is found to be near-Boltzmann, with an effective temperature of 1900 K. Using the Boltzmann plot to estimate the populations of higher energy states which were not measured in this work, we find that the remaining level of the ground-state multiplet ($^5D_0$, 975.1 cm^{-1}) is the only unmeasured state expected to exhibit any appreciable intensity (~2–3% of the total yield from the air-exposed surface). The populations of all higher states are negligible. Inclusion of the estimated $^5D_0$ yields (air-exposed and clean) into the data for Table 2 would lower the ground-state fractions by ~1%. The partitioning of the atoms removed from the clean substrate is not well described by the Boltzmann equation, but a least-squares analysis yields a temperature of 955 K. These values are substantially higher than the temperatures of 680 K (clean) and 840 K (air-exposed) obtained with a 900 eV ion beam.[15] The data are consistent with the results presented earlier in this paper, which indicate that excited-state fractions increase with incident ion kinetic energy. Further comparison can be made with the LIF data of Young *et al.*, who measured an effective temperature of 600 K for Fe under 3 keV Ar^+ ion bombardment[9] and Schweer and Bay who reported a temperature of 980 K for Fe desorbed from a steel matrix under 10 keV Ar^+ ion bombardment.[16] In addition, the increase in effective temperature with oxygen exposure has also been documented for other elements.[28] Note that 'temperature' is used as a convention for expressing the data in a convenient form. A Boltzmann distribution is not necessarily expected since ion-induced desorption is a non-equilibrium process.

The measured intensities and relative yields of ion-desorbed In species are presented in Table 3. The ion fractions are 0.13 and 3.8×10^{-3} for the contaminated and ion beam-cleaned surfaces, respectively. The corresponding ground-state neutral fractions are 0.72 and 0.92. The In^+ ion response drops by a factor of ~7 upon cleaning, despite the presumed exposure of more In atoms to the ion beam, while the ground-state atom yield increases approximately sevenfold. However, the large disparity in the magnitudes of the respective intensities discounts a one-for-one switch from ion to neutral ejection as the target is cleaned. Although the composition of the air-exposed sample studied here was not determined, the large increase in the ground-state yield may be partly attributed to an elevated absolute sputter yield.

The $In^*(^2P_{3/2})$ level is the only In excited state found with any appreciable intensity. Since a significant portion of this intensity is known to be the result of photodissociation of In_2°, the probability of which is unknown, calculation of a Boltzmann temperature would be dubious. This also means that the reported ground-state fraction must be considered as an upper bound. However, since both of the atoms originating from each dimer are detected at the 325.0 nm wavelength used to probe $In^*(^2P_{3/2})$, the In° useful fraction of Table 3 may be viewed as a reasonable estimate.[19]

As indicated earlier, the measured intensity for each electronic state is likely the result of a combination of effects. For example, direct population as a result of momentum transfer has been partially examined here in the context of the ion beam energy investigation. Cascading from higher energy levels into the state of interest may also occur. However, studies of highly energetic states have indicated very little populaton at energies of >2 eV above the ground state.[29,30] The measurements may also reflect the effects of non-radiative transitions from the measured metastable levels to the ground state. The mechanisms of these de-excitations are not entirely understood, but may be similar to those applied to ionization/neutralization. One theory relating de-excitation to the shielding of atomic levels from the conduction band of a metal has successfully described experimental observations for In and several other elements.[26] Finally, the influence of oxygen on excited-state fractions has been reviewed, although an accepted mechanism has not been established.[31]

CONCLUSION

The results of these measurements demonstrate several features of MPRI of ion-desorbed matter. First, the detectable fraction or useful fraction is influenced to some extent by the primary ion energy and the sample chemistry. Although the effect is typically small and predictable, the observations underscore the value of full characterization of the MPRI approach.

Second, when MPRI and SIMS are applied to analysis of the same chemical system, the improved quantitation available with MPRI is evident. This is illustrated by the extreme difficulty in correlating sec-

Table 4. Comparison of the factors which determine the useful yield for SIMS, MPRI and non-resonant MPI

	SIMS		MPRI		MPI	
	Air-exposed	Clean	Air-exposed	Clean	Air-exposed	Clean
Useful fraction[a]	0.11	3.8×10^{-3}	0.72	0.92	0.88	0.99
Ionization efficiency	1		1		1	
Spatial overlap[b]	1		0.47		1.6×10^{-2}	
Transmission[c]	0.10		0.10		0.10	
Useful yield	0.011	3.8×10^{-4}	0.033	0.043	1.3×10^{-4}	1.5×10^{-4}

[a] Useful fraction data are for indium (Table 3, MPI = $In^{\circ} + In^{*}$).
[b] Laser spatial overlap is calculated from data supplied in Ref. 2, using a 2.56 μs wide primary ion pulse.
[c] The transmission estimated for this apparatus (10%) is assigned to all three techniques, although the values for commonly employed SIMS instruments may be up to two orders of magnitude smaller. A unit detector efficiency is assumed.

ondary ion yields with surface concentration for In and Fe targets under 10 keV Ar^+ ion bombardment. The SIMS matrix effect is one of the primary motivations for applying MPRI to the analysis of solids. While the state selectivity of resonance ionization is also associated with a form of matrix effect, it is not a serious limitation and proves valuable for characterizing the ion–solid interaction.

Finally, the measurements of the useful fraction for MPRI of Fe and In demonstrate the inherent sensitivity of the MPRI technique. Combining the data with the remainder of the contributions to the useful yield, the latter quantity may be calculated for this experimental apparatus. The results are presented in Table 4. For comparison, the corresponding useful yields for SIMS and MPI are also calculated. It may be informative to view the air-exposed data as corresponding to bombardment of the surface with an O_2^+ ion beam, an approach often used for enhancing secondary ion yields. An equivalent transmission of 10% is assumed for both SIMS and MPRI in the computation, although significantly smaller values (0.1%) are typical for the magnetic sector or quadrupole-based instruments commonly employed for SIMS.[32] We find that the useful yields for MPRI and SIMS of a clean In surface are 0.043 and 3.8×10^{-4}, respectively. As a check, we cite a separate In determination carried out using this apparatus under slightly varied experimental conditions, in which the MPRI useful yield from a 'clean' surface was measured to be ~0.025. Even at this lower value, which results from a reduced spatial overlap between the laser and the desorbed atom reservoir (as compared with Table 4), a detection limit of 9 ppt was demonstrated.[1]

Non-resonant MPI may be used as a non-selective alternative to MPRI. This has proven to be useful, particularly in the case of survey analyses.[13,14] The useful fraction given for MPI in Table 4 is obtained by summing the measured In° and In^{*} fractional yields, while the spatial overlap factor is calculated by assuming a focused laser and using an approach described elsewhere.[6] Since this apparatus is well suited for non-resonant analyses, equivalent transmissions are assumed. Note that the useful yields for MPI do not suffer from substantial matrix effects. However, the small laser volume often required to ionize efficiently the many species results in detection limits roughly equivalent to those of SIMS.

Acknowledgements

The authors wish to thank F. M. Kimock for critical review of the manuscript and are grateful for the financial support of the National Science Foundation and the Office of Naval Research.

REFERENCES

1. D. L. Pappas, D. M. Hrubowchak, M. H. Ervin and N. Winograd, *Science* **243**, 64 (1989).
2. N. Thonnard, J. E. Parks, R. D. Willis, L. J. Moore and H. F. Arlinghaus, *Surf. Interface Anal.* **14**, 751 (1989).
3. M. J. Pellin, C. E. Young, W. F. Calaway and D. M. Gruen, *Nucl. Instrum. Methods Phys. Res.* **B13**, 653 (1986).
4. J. E. Parks, M. T. Spaar and P. J. Cressman, *J. Cryst. Growth* **89**, 4 (1988).
5. C. E. Young, M. J. Pellin, W. F. Calaway, B. Jorgensen, E. L. Schweitzer and D. M. Gruen, *Nucl. Instrum. Methods* **B27**, 119 (1987).
6. F. M. Kimock, J. P. Baxter, D. L. Pappas, P. H. Kobrin and N. Winograd, *Anal. Chem.* **56**, 2782 (1984).
7. C. W. White, D. L. Simms and N. H. Tolk, *Science* **1077**, 481 (1972).
8. M. L. Yu, D. Grischkowsky and A. C. Balant, *Phys. Rev. Lett.* **48**, 427 (1982).
9. C. E. Young, W. F. Calaway, M. J. Pellin and D. M. Gruen, *J. Vac. Sci. Technol. A* **2**, 693 (1984).
10. R. E. Honig, in *Advances in Mass Spectrometry*, ed. by R. M. Elliott, p. 25. Pergamon, Oxford (1963).
11. H. Oechsner and W. Gerhard, *Surf. Sci.* **44**, 480 (1974).
12. J. W. Coburn, E. Taglauer and E. Kay, *J. Appl. Phys.* **45**, 1779 (1974).
13. C. H. Becker, *J. Vac. Sci. Technol. A* **5**, 1181 (1987).
14. C. H. Becker and K. T. Gillen, *J. Vac. Sci. Technol. A* **3**, 1347 (1985).
15. F. M. Kimock, D. L. Pappas and N. Winograd, *Anal. Chem.* **57**, 2669 (1985).
16. B. Schweer and H. L. Bay, *Vides Couches Minces* **201**, 1349 (1980).
17. M. J. Pellin, R. B. Wright and D. M. Gruen, *J. Chem. Phys.* **74**, 6448 (1981).
18. F. M. Kimock, J. P. Baxter, D. L. Pappas, P. H. Kobrin and N. Winograd, in *Analytical Spectroscopy, 26th ORNL Conference on Analytical Chemistry in Energy Technology, Knoxville, 1983*. Elsevier, New York. Ed. by W. S. Lyon (1984).
19. D. L. Pappas, D. M. Hrubowchak, M. H. Ervin and N. Winograd, in preparation.
20. F. M. Kimock, J. P. Baxter and N. Winograd, *Surf. Sci.* **124**, L41 (1983).
21. B. A. Mamyrin, V. I. Karataev, D. V. Schmiik and V. A. Zagulin, *Sov. Phys. JETP* **37**, 45 (1973).
22. C. H. Becker and K. T. Gillen, *Anal. Chem.* **56**, 1671 (1984).

23. N. Winograd, in *Progress in Solid State Chemistry*, ed. by C. M. Rosenblatt and W. L. Worrell, p. 285. Pergamon, Oxford (1981).
24. W. Gerhard and H. Oechsner, *Z. Phys. B* **22**, 41 (1975).
25. N. Winograd, K. E. Foley, B. J. Garrison and D. E. Harrison, Jr., *Phys. Lett.* **73A**, 253 (1979).
26. B. I. Craig, J. P. Baxter, J. Singh, G. A. Schick, P. H. Kobrin, B. J. Garrison and N. Winograd, *Phys. Rev. Lett.* **57**, 1351 (1986).
27. R. Behrisch, J. Roth, J. Bohdanski, A. P. Martinelli, B. Schweer, D. Rusbuldt and E. Hintz, *J. Nucl. Mater.* **93/94**, 645 (1980).
28. M. J. Pellin, C. E. Young, M. H. Mendelsohn, D. M. Gruen, R. B. Wright and A. G. DeWald, *J. Nucl. Mater.* **111/112**, 738 (1982).
29. R. W. Hewitt and N. Winograd, *J. Appl. Phys.* **51**, 2620 (1980).
30. M. J. Pellin, D. M. Gruen, C. E. Young and M. D. Wiggins, *Nucl. Instrum. Methods Phys. Res.* **218**, 771 (1983).
31. D. M. Gruen, M. J. Pellin, C. E. Young and M. H. Mendelsohn, *Phys. Scr.* **T6**, 42 (1983).
32. G. Betz, *Nucl. Instrum. Methods Phys. Res.* **B27**, 104 (1987).
33. R. J. Colton, J. E. Campana, T. M. Barlak, J. J. DeCorpo and J. R. Wyatt, *Rev. Sci. Instrum.* **51**, 1685 (1980).